HLPW-4/GMGW-3: Overview and Workshop Summary

Christopher L. Rumsey*
NASA Langley Research Center

Jeffrey P. Slotnick†
The Boeing Company

Carolyn D. Woeber‡
Cadence Design Systems

The Fourth AIAA CFD High Lift Prediction Workshop and the Third Geometry and Mesh Generation Workshop were held collaboratively with the common goal of assessing the numerical prediction capability of current-generation computational fluid dynamics (CFD) technology for swept, medium/high-aspect-ratio wings in high-lift configurations. A key aspect of this joint endeavor was the use of Technology Focus Groups, an innovative new approach for workshops involving close collaboration between participants. These groups, which included both mesh-generation and flow-solver experts, worked to accelerate advancements for their particular methodologies by addressing key questions of importance *prior* to the workshop. The high-lift version of the NASA Common Research Model (CRM-HL) configuration was the focus of this workshop. Measured experimental wind-tunnel data were available for comparison. The workshop also included a two-dimensional turbulence model verification exercise based on the CRM-HL wing shape. Altogether, 44 participants submitted a total of 184 data sets of CFD results. This paper provides a high-level summary of the results and conclusions from the workshop. Like at past workshops, fixed-grid Reynolds-averaged Navier-Stokes continued to be inaccurate and inconsistent for high lift. However, mesh adaptation definitively brought more consistency. Scale-resolving methods appeared most promising for predicting high-lift flow physics.

I. Introduction

The fourth AIAA CFD High Lift Prediction Workshop (HLPW-4) [1] and third AIAA Geometry and Mesh Generation Workshop (GMGW-3) [2] were held jointly in San Diego, California in January 2022, in association with AIAA SciTech. The purpose of the HLPW series, which started in 2010, is to advance the state of the art in predicting high-lift flows with CFD software. The purpose of the GMGW series, started in 2017, is to identify, understand, and advance improvements in geometry and mesh-generation technology for CFD in aircraft and spacecraft systems. Current CFD technology for the prediction of low-speed, high-lift flowfields is generally considered unreliable and inconsistent. The reasons for these deficiencies are not fully known, but the interplay between flow-solver numerics, models, and meshing has drawn the interest of both the HLPW and GMGW communities. It is believed that more rapid advancement may be achieved by regularly bringing together an international group of experts from these communities.

The long-term objectives of the HLPW series are: (1) assess the numerical prediction capability (meshing, numerics, turbulence modeling, high-performance computing requirements, etc.) of current-generation CFD technology/codes for swept, medium-to-high-aspect ratio wings for landing/takeoff (high-lift) configurations; (2) develop practical modeling guidelines for CFD prediction of high-lift flowfields; (3) determine the elements of high-lift flow physics that are critical for modeling to enable the development of more accurate prediction methods and tools; and (4) enhance CFD prediction capability for practical high-lift aerodynamic design and optimization. The HLPWs make

*Research Scientist, Computational AeroSciences Branch, AIAA Fellow.
†Technical Fellow, Boeing Commercial Airplanes, AIAA Associate Fellow.
‡Director, Application Engineering, AIAA Associate Fellow.

use of configurations for which the geometry and measured data are fully open (with unrestricted public availability), forming the basis for international cooperation/collaboration. In keeping with the goals of the HLPW series, CFD data generated by workshop participants are also made publicly available. Regarding geometry and mesh-generation software, in addition to the goal of assessing the current state-of-the art, the GMGW series seeks to identify and develop understanding of areas needing improvement (performance, accuracy, applicability) as well as to provide a foundation for documenting best practices.

Summary papers covering the previous three HLPWs [3–5] describe the particular test cases and overall results. Summaries of the previous GMGWs are also available [6, 7]. There have also been many associated AIAA conference and journal papers written by workshop participants. The summary papers mentioned above include references to many of them. Over the course of the HLPWs to date, Reynolds-averaged Navier-Stokes (RANS) CFD methods have been the most common technology employed. Increasing computational capacity has allowed generally finer CFD meshes to be used in successive workshops, with improved geometric fidelity (including more geometric details, such as accurately-rendered slat bracket and flap fairing hardware) and greater flowfield resolution. Despite these improvements, RANS CFD has remained unreliable near $C_{L,max}$ at all workshops. Although individual RANS contributions could be found that agreed very well with measured lift coefficients near $C_{L,max}$, they typically achieved agreement for the wrong reasons. In HLPW-3, RANS separation patterns usually indicated much larger outboard separation and smaller inboard separation than indicated by oil flow patterns from wind tunnel tests.

The workshops have endeavored to uncover root causes to the inconsistent predictions by a variety of strategies, including the creation of common workshop meshes, collecting greater amounts of data (such as iterative convergence histories and velocity profiles), and conducting verification exercises. Although important issues have been identified by these efforts (for example, only 30% of the CFD codes passed the verification exercise for the Spalart-Allmaras (SA) [8] turbulence model in HLPW-3), the overarching problems with CFD near $C_{L,max}$ have remained. Efforts within HLPW-3 also encouraged the use of both mesh-adaptation and scale-resolving technologies to attack the problem. Although there was only limited participation in these areas, some positive benefits were seen. In particular, scale-resolving Lattice-Boltzmann (LB) methods used by two different groups indicated improvement over RANS in matching high-lift separation patterns. Although mesh adaptation did not yield definitive improvements at the time of HLPW-3, the strong influence of the mesh near $C_{L,max}$ made clear the importance of continuing to develop and promote this technology.

In all previous workshops, participants essentially worked independently, then brought their final results to the workshop, at which time they were compared collectively. For HLPW-4/GMGW-3, a different approach was taken in an effort to accelerate progress. Six Technology Focus Groups (TFGs) were formed well in advance of the workshop. The TFGs covered both the traditional areas of Geometry Modeling and Preparation for Meshing (GEOM) and Fixed-Grid RANS (RANS), as well as the newer areas of High-Order Discretization (HO), Mesh Adaptation for RANS (ADAPT), Hybrid RANS/Large-Eddy Simulation (HRLES), and Wall-Modeled Large-Eddy Simulation and Lattice-Boltzmann (WMLESLB). Members of these groups (both active and observers) met regularly, discussed their progress, shared their results, and planned their group's ongoing efforts. Then, at the workshop itself, rather than individual participants presenting their results, the TFG leaders gave summaries of their group's collective work over the preceding year. Most of these six TFGs have provided companion summary papers [9–13] that complement the current paper. Two other papers highlight the immense effort that went into RANS-based meshing for HLPW-4/GMGW-3 [14, 15]. It should also be noted that several individual participant papers on results from HLPW-4/GMGW-3 have already come out [16–21], with many more (not listed here) to appear at AIAA Aviation 2022.

HLPW-4/GMGW-3 also introduced the idea of reporting and highlighting technical progress through addressing Key Questions (KQs). KQs were devised by each TFG early in their formation, to provide goals to work toward. Specifically answering the KQs would bring everyone further along in the quest to improve geometry modeling, mesh generation, and CFD predictions for high-lift configurations. Toward the end of the current paper, a summary and status of high-level KQs from HLPW-4/GMGW-3 will be described.

HLPW-4/GMGW-3 made use of the high-lift Common Research Model (CRM-HL) [22, 23]. This publicly-available configuration forms a major component of an ecosystem of coordinated wind tunnel testing and experimentation that is underway to enable users around the globe to collaborate, explore, and document high-lift flow physics for the purpose of validating and improving CFD analysis and design capability. Improving the prediction of high-lift flows is a key to enabling certification by analysis, which would significantly reduce the cost of bringing new aeronautical products to market [24]. As more and more test data are acquired within the CRM-HL ecosystem, additional HLPWs are planned to continue on a regular schedule to address ongoing gaps and shortcomings in CFD predictive capability. This interplay will encourage greater synergy between the wind-tunnel testing and CFD development.

The particular CRM-HL test article used was the 10%-scale NASA semispan model [25], tested in the QinetiQ

wind tunnel in the UK in 2019 [26]. As described below, HLPW-4/GMGW-3 focused on the landing configuration with slat angle at 30° and flap angles set at 40° inboard and 37° outboard, although Test Case 1 also investigated the effect of changing the flap angle at low-lift conditions.

It is important to mention that the current paper looks at results across *all* the TFGs, searching for trends, documenting lessons learned, and addressing the overall status of CFD predictive capability. The reader is referred to the individual TFG summary papers mentioned above for more details on each specific technology subject.

II. Test Cases and CFD Meshes

The test cases, defined on the workshop's website [1], are summarized here. Note that the GEOM TFG dealt with very different test cases, which are not covered in this paper at all. For all CRM-HL cases (Test Cases 1 and 2), the conditions were: $M = 0.2$, $Re_{MAC} = 5.49 \times 10^6$, $T = 521^\circ R$, $p = 24.67$ psi. The geometry was provided in full-scale inches. The configuration was provided "as designed;" there was no effort to measure or compute the "as-tested" aeroelastic shape(s) of the semispan wall-mounted test article for this workshop.

The mean aerodynamic chord (MAC) was 275.8 inches, the moment reference center was at $x = 1,325.9$, $y = 0$, and $z = 177.95$ inches, and the semispan model reference area was $297,360$ inches^2. Participants were requested to run the cases "fully turbulent" (no transition specified). In the QinetiQ wind tunnel, the model was tripped (using trip dots) in several regions believed to have laminar flow: near the wing leading edge outboard of the slat, on the wing insert over the pylon, on the wing root strake inboard of the slat, near the front of the nacelle and pylon, and near the fuselage nose. A picture of the CRM-HL configuration (from the CFD) is shown in Fig. 1. The configuration includes a nacelle/pylon with a vorticity-producing chine on the upper surface of the nacelle. There are 12 slat brackets attaching the outer slat element to the main wing, 3 slat brackets attaching the inner slat element to the main wing, and 3 flap fairings covering the attachments between the flap and the main wing.

Figure 1. The CRM-HL configuration.

A. Test Case 1: Flap Deflection Study

In Test Case 1a, participants were asked to solve for the flow over the CRM-HL in free air at the corrected angle of attack of $\alpha = 7.05^\circ$, using three different flap settings: $40^\circ/37^\circ$ inboard/outboard (nominal configuration), $37^\circ/34^\circ$, and $43^\circ/40^\circ$. This angle of attack is not near $C_{L,max}$; it is in the linear portion of the lift curve. The goal was to assess the accuracy of predictions of the flap setting effects on forces and moment to compute increments due to flap deflection.

In Test Case 1b, flow solutions were sought at $\alpha = 7.05^\circ$ for the nominal flap setting on a series of consistently refined fixed meshes. The goal was to assess mesh convergence properties.

B. Test Case 2: $C_{L,max}$ Study

Test Case 2 uses the nominal flap setting only. In Test Case 2a, free air computations were requested at the following corrected angles of attack: 2.78, 7.05, 11.29, 17.05, 19.57, 20.55, and 21.47 degrees. In the corrected wind tunnel

data, $C_{L,max}$ occurs near $\alpha = 18.5 - 19°$.

In Test Case 2b, in-tunnel computations were requested (with the test article mounted on the floor of the QinetiQ tunnel) at the following uncorrected angles of attack: 1.99, 5.98, 9.98, 15.48, 17.98, 18.97, and 19.98 degrees. The uncorrected $C_{L,max}$ occurs near $\alpha_u = 17.5°$.

C. Test Case 3: Turbulence Model Verification Study

The configuration used in the verification test case was a simplified two-dimensional (2-D) multielement airfoil configuration, as documented on the NASA Langley Turbulence Modeling Resource (TMR) website [27]. This same configuration was used for the 2020 AIAA Aviation GMGW Special Session (see, for example, Refs. [28, 29]). The main purpose of this exercise was to demonstrate accurate and consistent implementation of the SA turbulence model (with freestream conditions of the turbulence variable set to $\hat{\nu}_{freestream}/\nu_\infty = 3$) used in conjunction with RANS (the variants SA-neg and SA-noft2 are also considered applicable [30]). The test conditions were: $M = 0.2$, $Re = 5 \times 10^6$ based on stowed chord length, $T = 272.1$ K, and $\alpha = 16°$.

D. CFD Meshes

Nearly 170 different CRM-HL meshes were created and submitted in support of HLPW-4/GMGW-3; some of these were created by the workshop committee, and some were created by participants. A set of mesh-generation guidelines was provided prior to the workshop [1]. These guidelines were based on prior workshop experience with fixed-grid RANS solvers, and they included specification of desired minimum spacings at walls in terms of the inner-law variable y^+_{min}. These RANS-based guidelines were not necessarily appropriate for the HO, ADAPT, HRLES, or WMLESLB TFGs. During the course of the workshop preparation, the TFGs explored and refined their own best practices for mesh generation. Some information can be found in their respective summary papers [10–13].

Graphical summaries of the committee-generated free-air mesh sizes created for RANS are provided in Fig. 2. In comparison with the CRM-HL mesh sizes from HLPW-3 [5], these meshes were roughly similar in terms of point count, with level A corresponding to coarse, B to medium, C to fine, and D to extra fine.[a] The meshes were designed with the expectation that the D-level meshes would be appropriate for best-practice usage, with coarser A through C levels and finer E level used for mesh-convergence studies. However, it turned out that, due to insufficient computational resources, many participants were unable to routinely run on the C- and D-level meshes. Therefore, the planned E-level meshes were never created.

CRM-HL meshes have been made available to the public, and posted to the HLPW website [31]. The meshes include those believed to be appropriate for fixed-grid RANS as well as others (created by participants) for HO, HRLES, and WMLES. Some participant meshes that include the QinetiQ wind tunnel (for in-tunnel computations) are also available. Meshes for off-nominal flap angles are also posted. Additional details about the meshes are not given here, but can be found in a summary document available on the HLPW website.

III. Summary of Entries

In this section, a broad overview of the workshop participation is given. It it important to reiterate that each TFG had both active participants as well as observers. Therefore, only a small percentage of the TFG members ended up submitting data for the workshop. Nonetheless, this workshop had far more data submissions than any of the earlier workshops in the series: altogether, 44 groups submitted 184 entries. (In HLPW-1, 21 groups submitted 39 entries; in HLPW-2, 26 groups submitted 48 entries; in HLPW-3, 35 groups submitted 79 entries.) The entries are summarized in Table 1, where the particular TFG is denoted in the entry number by a letter: R=RANS, H=HO, A=ADAPT, L=HRLES, and W=WMLESLB. (Note that only one of the entries in the WMLESLB TFG used Lattice-Boltzmann (LB). Most of the others used WMLES. However, two of the entries were unique: one solved the Euler equations – i.e., fluid viscosity was not modeled – in combination with mesh adaptation, and one solved WMLES with a high-order scheme.) Each participant was asked to denote one or more of their entries as "best practice" (BP) in order to clarify which of their data should be highlighted in workshop comparisons (other data submitted may have been on coarser meshes, may have been incomplete, or may have used different non-optimal code settings as part of parametric CFD studies). The test cases covered by the participants in their BP results are designated with a "Y" in the table. Note

[a]Note that for the overset meshes [15], the sizes are given in terms of solution nodes only, and the number of solution cells is taken to be approximately the same as the number of solution nodes. Also note that one of the overset meshes, designated 4, explored level A mesh size with a finer minimum spacing at walls: nominally $y^+_{min} = 1.0$. The unstructured family 2 was the same as family 1 except they were smoothed in a postprocessing step. Mesh family 5.3 was similar to family 2.3, with fixes made in slat-bracket and flap-track-fairing regions [14].

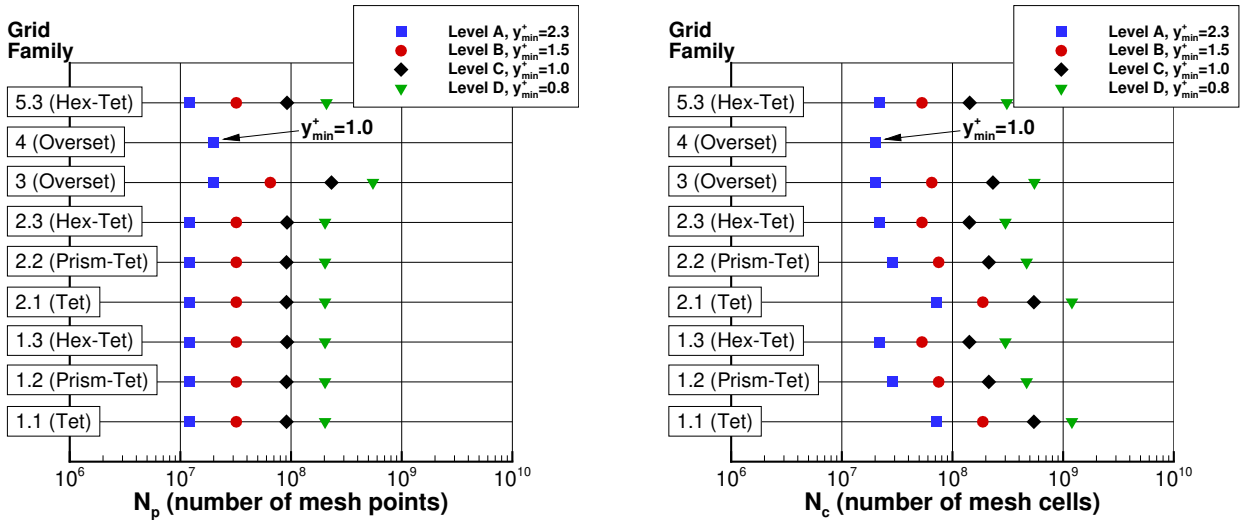

(a) Mesh points

(b) Mesh cells

Figure 2. Summary of HLPW-4/GMGW-3 committee meshes (designed for RANS).

that the Test Case 3 verification exercise was designed for RANS solutions only (covered by RANS, HO, and ADAPT TFGs). As mentioned earlier, this paper does not describe the work performed in the GEOM TFG.

IV. Spalart-Allmaras Turbulence Modeling Verification Results

Code verification is known to be a crucial step prior to conducting validation activities [32]. The purpose of verification is to insure that a CFD code has implemented a given mathematical model correctly (i.e., no coding mistakes or undocumented aspects or additions). Without verification, drawing firm conclusions about model accuracy at workshops becomes impossible because the CFD results are not necessarily obtained using consistent turbulence models between different codes. Because the SA turbulence model for RANS is used by so many participants for high-lift applications, Test Case 3 focused on a verification exercise for that particular model, using a benchmark numerical solution of a multielement airfoil from the TMR website [30]. The use of a benchmark solution is typically a necessary (but not sufficient) measure of verification. In other words, reasonable agreement with a benchmark solution does not guarantee that the code is free from mistakes, whereas clear disagreement with a benchmark solution *does* indicate a problem. This section summarizes the Test Case 3 results from all RANS-type entries (RANS, HO, and ADAPT).

Figure 3 shows lift, pressure drag, and viscous drag coefficients predicted by the participants on successively finer meshes ($h \to 0$). As the mesh is refined, the various solutions should approach the same infinite-mesh result (roughly indicated in the figure by a pink circle located at $h = 0$). For the most part, the submissions appeared to be consistent here. Note that on a given finite mesh, there may be significant differences between solutions because of different methodologies, discretization schemes, etc. In fact, it is clear that for a given h, the HO (light blue) and ADAPT (dark blue) solutions were typically more accurate than the RANS (red) results, as expected. But as long as a given solution is approaching the "benchmark" result as $h \to 0$, the coding of the model is (likely) implemented correctly. As seen in the figures, a few solutions stand out. H-012 trended away from the accepted C_L solution and was far away from $C_{D,v}$. R-059.2 did not appear to be trending accurately toward $C_{D,p}$ [b]. Finally, the $C_{D,v}$ of R-054.1 appeared to be trending slightly away from the benchmark solution on its finest mesh.

Looking solely at the force coefficient trends is rarely definitive on its own. It is also helpful to look at flowfield profiles and surface quantities. In Fig. 4, profiles of u/U_{ref} and μ_t/μ_{ref} from the finest meshes are examined at one location on the main element (other locations were examined at the workshop, but are not shown because they lead to similar conclusions). Again, H-012 and R-059.2 stand out, trending away from the collective results. However, note that the eddy viscosity in the wake region (Fig. 4(b)) tended to be inconsistent among most of the RANS (red) results. On the other hand, the HO (light blue) and ADAPT (dark blue) results produced results that were nearly on top of each

[b]R-059.2 had the same turbulence model coding as R-059.1, which appeared to be accurate. However, R-059.2 used a custom spatial accuracy setting lower than second order, which was therefore the most likely cause of the inconsistent behavior.

Table 1. Summary of HLPW-4/GMGW-3 Entries.

Entry number	Primary organization	Code name	Total number of entries	"Best practice" (BP) entries	BP cases: 1a	1b	2a	2b	Case 3
R-004	JAXA	TAS	5	1	Y	Y	-	-	Y
R-008	NASA LaRC	FUN3D	6	1	Y	Y	Y	-	Y
R-009	Hexagon	scFLOW	5	1	-	-	Y	-	-
R-011	Indian Inst. Sci.	HiFUN	2	2	-	Y	Y	-	Y
R-015	NASA LaRC	USM3D	4	1	Y	Y	Y	-	Y
R-019	Embraer	CFD++	15	1	-	-	Y	-	Y
R-021	Zenotech	zCFD	3	1	Y	-	-	-	Y
R-025	NASA Ames	LAVA	13	1	Y	Y	Y	Y	Y
R-028	ICUBE	NSMB	4	1	-	-	Y	-	-
R-032	Seoul Nat. U.	ACTFlow	1	1	-	Y	Y	-	Y
R-034	Poly. Montreal	CHAMPS	9	1	-	Y	Y	-	Y
R-037	Boeing	OVERFLOW	9	4	Y	Y	Y	-	-
R-043	ARA	TAU	12	2	Y	-	Y	-	Y
R-050	TU Braunschweig	TAU	1	1	Y	-	Y	-	Y
R-054	QinetiQ	Fluent	3	1	-	-	Y	-	Y
R-057	Kawasaki Heavy	Cflow	6	1	-	Y	Y	-	Y
R-059	Siemens	STAR-CCM+	9	2	-	-	Y	-	Y
R-060	Flexcompute	Flow360	10	1	Y	Y	Y	-	Y
H-004	MIT	SANS	3	2	-	-	-	-	Y
H-005	U. Tennessee	Kestrel/COFFE	3	3	-	-	-	-	Y
H-012	ONERA	NXO CC-CV	1	1	-	Y	Y	-	Y
H-013	Princeton	maDG	2	1	Y	Y	Y	-	-
H-023[1]	Boeing	GGNS-T1	1	0	-	Y	-	-	-
A-002	INRIA	Wolf	1	1	-	Y	Y	-	Y
A-004	NASA LaRC	FUN3D	4	2	Y	Y	Y	-	Y
A-013	MIT	SANS	2	1	-	-	-	-	Y
A-025	Boeing	GGNS-T1+EPIC	3	2	Y	Y	Y	-	Y
A-026	Istanbul Tech. U.	HEMLAB+PyAMG	1	1	Y	Y	Y	-	Y
A-031	U. Tennessee	Kestrel/COFFE	1	1	-	-	Y	-	-
L-001	Amazon	CFD++	10	2	-	-	Y	Y	n/a
L-004	Virgin Galactic	FUN3D	2	1	Y	-	-	-	n/a
L-005	U. Tennessee	Kestrel/KCFD	1	1	Y	-	-	-	n/a
L-016	NASA Ames	LAVA	7	1	-	-	Y	-	n/a
L-038	DLR	TAU	1	1	-	-	Y	-	n/a
L-053	Kawasaki Heavy	Cflow	2	1	-	-	Y	-	n/a
W-020	NASA Ames	LAVA	5	1	-	-	Y	Y	n/a
W-021	Stanford	charLES	4	1	-	-	Y	Y	n/a
W-030[2]	KTH	Euler Real Flight Sim	1	1	-	-	Y	-	n/a
W-031	Boeing	BCFD	1	1	-	-	Y	-	n/a
W-032[3]	Dassault Sys.	PowerFLOW	1	1	Y	Y	Y	Y	n/a
W-034	BSC	Alya	4	1	-	-	Y	-	n/a
W-047[4]	U. Kansas	hpMusic	1	1	-	-	Y	-	n/a
W-049	Tohoku U.	FFVHC-ACE	2	1	-	-	Y	-	n/a
W-050	NASA LaRC	FUN3D	3	1	-	-	Y	-	n/a

[1] only one datapoint provided; [2] Euler with adaptive meshing; [3] Lattice-Boltzmann; [4] high-order scheme

other. The reason for this difference is that the finest meshes were still not refined enough in the wakes to sufficiently reduce the local discretization errors in standard RANS solvers, but high-order and adaptive methods were better able to resolve the flow there. Note that zoomed plots of the eddy-viscosity profiles (not provided here) showed that a few of the RANS participants (R-021.1, R-019.1, R-043.1) used somewhat higher-than-requested freestream levels of the SA turbulence variable (the Test Case specified $\hat{\nu}_{freestream}/\nu_\infty = 3$). The effects of this difference on the resulting turbulence in the boundary layer are not known, although it appeared to have no perceptible impact.

Figure 5 shows surface pressure coefficients and the x-component of surface skin friction coefficient, zoomed in to specific regions. On the flap, the entries R-057.3 and and H-012 yielded deviations in C_p from the collective. Over the main element, H-012 produced large deviations in $C_{f,x}$, whereas the entries R-054.1 and R-059.2 yielded smaller deviations over the front of the element. The other results agreed well with each other, although some of the HO results exhibited high-frequency oscillations that were not plotted here.

Overall, then, the SA model verification exercise proved to be successful for most participants. Of those results submitted, a few minor issues still should be addressed in R-054.1 and R-057.3, and oscillations in $C_{f,x}$ in some of the HO results have been noted. Otherwise, all except H-012 and R-059.2 produced solutions that appeared to be acceptably approaching the benchmark (collective) solution. The failure of R-059.2 was likely due to setting the spatial accuracy of the solver to be less than second order for that particular solution. This success rate of nearly 100% is a dramatic improvement from HLPW-3, when only 30% passed the verification exercise.

V. CRM-HL Workshop Results

This section provides an overview of the workshop results that made use of the CRM-HL configuration. The subsections focus on various specific studies, including mesh convergence, flap deflection, and maximum lift. Following from the previous HLPWs, a statistical analysis of the submitted data is also performed. Iterative convergence and velocity profiles are also briefly explored. It should be noted that far more data were submitted to HLPW-4/GMGW-3 than has been possible to analyze. However, all data are available on the workshop website, so more analysis can be independently performed in the future.

A. Mesh Convergence Study

In Test Case 1b, participants were asked to provide solutions for the nominal configuration at $\alpha = 7.05^\circ$. Because most of the participants who did this case used the SA turbulence model, we focus only on those results here, and also make use of the verification results from the last section.

Figure 6 shows lift coefficient as a function of h, which is a measure of mesh spacing. As $h \to 0$, the mesh spacing gets finer, and it is expected that all solutions using a given turbulence model should approach the same result. All SA results are shown in Fig. 6(a), while only results from those codes that demonstrated SA verification are shown in Fig. 6(b). Because so many of the participants who submitted Test Case 3 results appeared to be verified for SA, the latter plot only removed 3 solutions. In the end, the verified SA results ended up with only slightly tighter clustering as $h \to 0$. And the RANS and ADAPT solutions tell somewhat different stories. Whereas the ADAPT solutions appeared to be generally heading toward a C_L near $1.765 - 1.78$ (indicated by a dashed blue line along the left side of Fig. 6(b)), it is unclear where the verified SA RANS solutions were heading as $h \to 0$. The infinite-mesh RANS solution appeared to be somewhere in the range of the dashed red line highlighted by the question mark, between around $1.73 < C_L < 1.77$. While this range includes much of the apparent approximate infinite-mesh ADAPT solution range, many of the individual RANS submissions certainly did not appear to be heading in that direction. Presumably, if all the codes were indeed verified (and if iterative convergence was not an issue), most of these remaining differences between fine-mesh solutions would be due to discretization errors. In other words, this mesh-convergence study, combined with the results from the verification exercise, indicates that additional refinement of the fixed meshes far beyond the current levels would be required to bring the solutions closer together.

These results highlight the importance of verification, which can provide greater confidence that disagreements between codes are primarily due to discretization errors, and not to any differences in model implementation. However, they also draw attention to the importance (and difficulty) of running on sufficiently fine fixed meshes for complex 3-D configurations like the CRM-HL. On the other hand, adaptive meshing, which automatically provides more resolution where it is needed, appeared to be able to achieve solutions that were closer to mesh-converged.

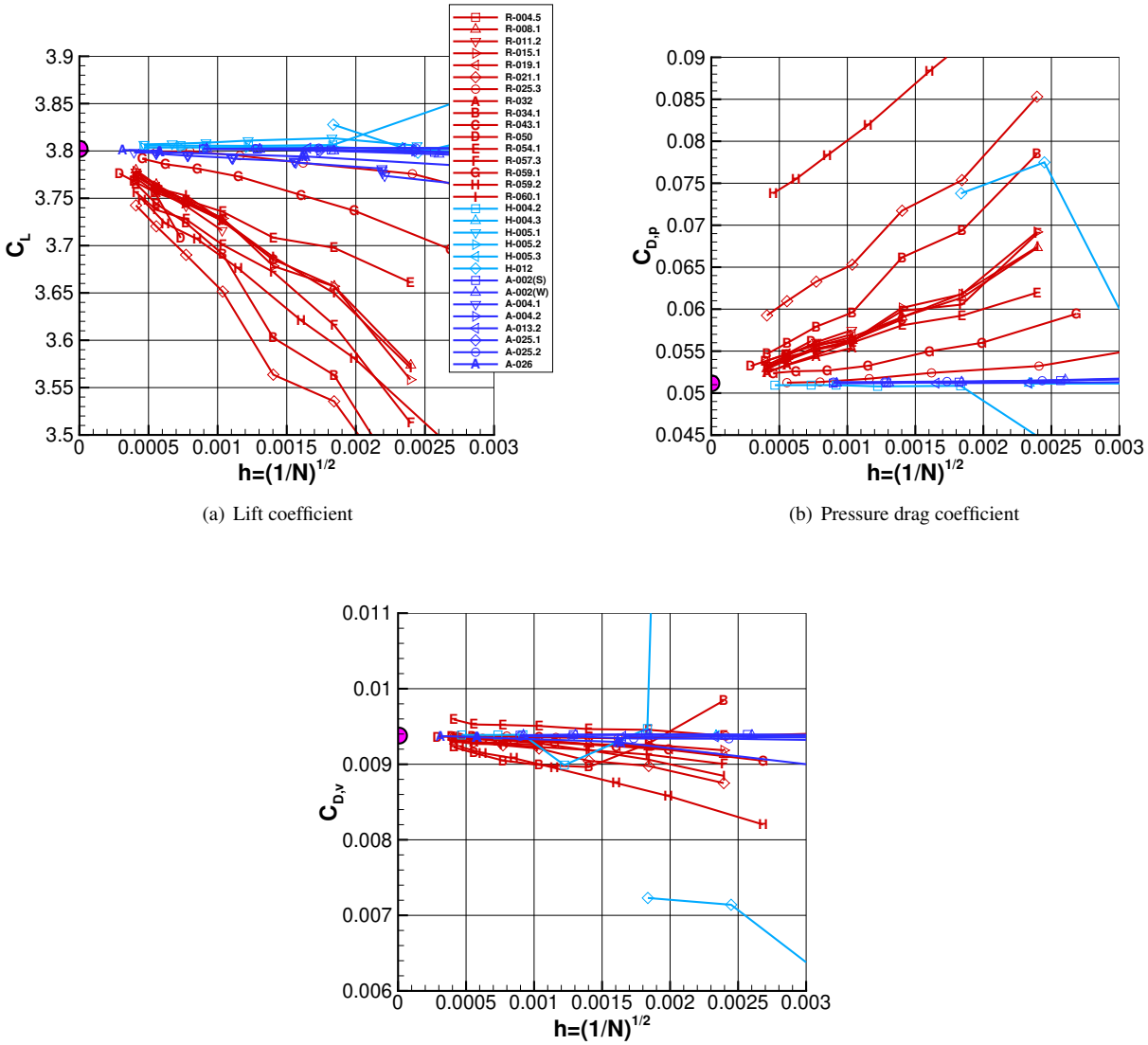

(a) Lift coefficient

(b) Pressure drag coefficient

(c) Viscous drag coefficient

Figure 3. Case 3 mesh convergence, SA turbulence model.

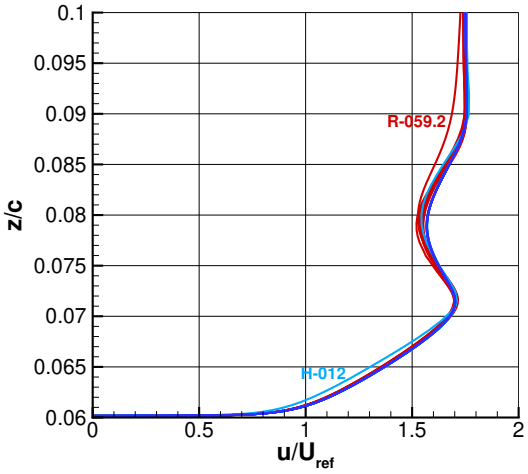

(a) Main element u/U_{ref} at $x/c = 0.40$

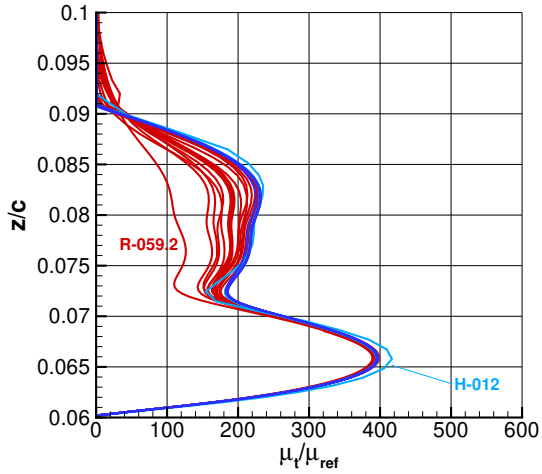

(b) Main element μ_t/μ_{ref} at $x/c = 0.40$

Figure 4. Case 3 profiles, SA turbulence model.

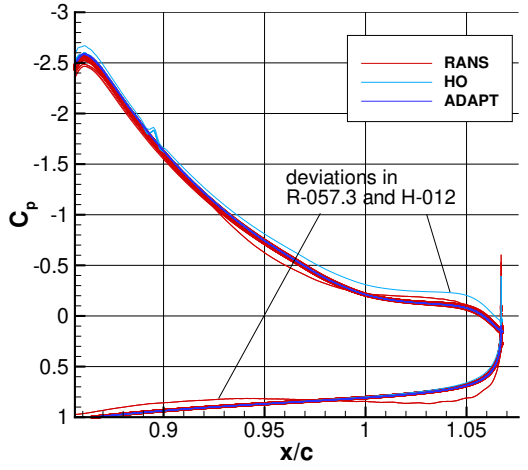

(a) Surface pressure coefficient on flap element

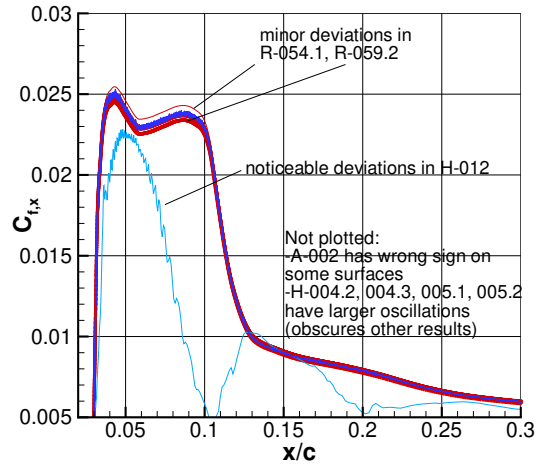

(b) x-component of surface skin friction coefficient on front upper surface of main element

Figure 5. Case 3 surface coefficients, SA turbulence model.

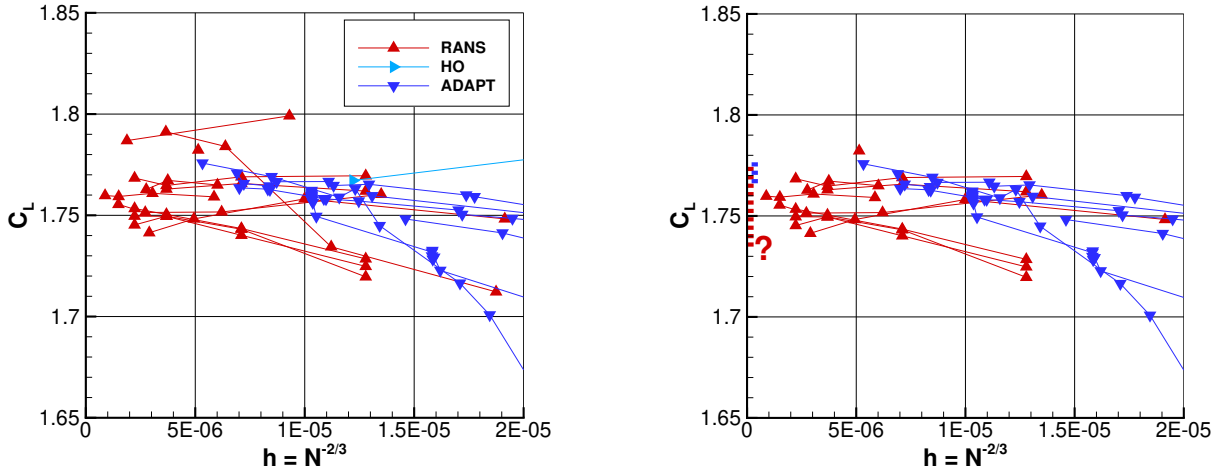

(a) All SA results

(b) Verified SA results

Figure 6. Mesh convergence of CRM-HL lift coefficient at $\alpha = 7.05°$, SA turbulence model.

B. Flap Deflection Study

Here, and for the remainder of the paper (unless otherwise noted), we only show submitted results denoted as "best practice" (BP) by the participants. Results from Test Case 1a, the flap deflection study, are shown in Fig. 7. Figure 7(a) plots C_L as a function of the inboard flap angle. Observed from the wind-tunnel measurements, the CRM-HL configuration lift continues to increase as the flap angle increases. On the other hand, most of the CFD results indicate increasing lift between inboard flap angles of $37°$ and $40°$, but decreasing lift between $40°$ and $43°$. Figure 7(b) shows the CRM-HL pitching moment coefficient for BP submissions. These also generally indicate the wrong trend between the two larger flap angles.

In Fig. 7(c), the three participant results that came closest to predicting the correct C_L increment trends are highlighted. Two of these were fixed-grid RANS results and one was a Lattice-Boltzmann result from the WMLESLB TFG. In Fig. 7(d), the pitching moment coefficients are shown for the selected results that yielded the best predictions of lift. Among these, only W-032 exhibited a somewhat similar trend as the wind tunnel measurements. The two RANS results were poor, similar to other RANS trends for $C_{m,y}$.

Looking at surface streamline patterns in Fig. 8, it is evident that the W-032 result (Fig. 8(b)) predicted less outboard flap separation than the typical RANS result (Fig. 8(a) shows R-025.3). The reduced flap separation was in generally better agreement with the oil flow photograph (Fig. 8(c)). (Note that the image files used in the comparisons were submitted directly to the workshop by the participants; no effort was made to modify or control the image lighting, resolution, or other details.) However, although not shown, even the W-032 result that seemed to agree best with *both* C_L and $C_{m,y}$ trends tended to underpredict the peak suction on the main and flap elements.

C. Maximum Lift Study

The force and moment polars predicted by the CFD are shown in Fig. 9, along with experimental measurements. Test Case 2a (Figs. 9(a), (c), and (e)) were free-air computations, and are compared with corrected test data. Test Case 2b (Figs. 9(b), (d), and (f)) were in-tunnel computations, and are compared with uncorrected test data. Among the Case 2a results, a large scatter of results near $C_{L,max}$ is seen. This inconsistency has also occurred at previous HLPWs, for different high-lift configurations. It is more difficult to draw conclusions about the Case 2b results because there were only five entries. However, these all agreed very well with the uncorrected measured force data.

It is clear from the Fig. 9(a) that many of the RANS (red) solutions lost significant lift near $C_{L,max}$. In spite of this, there were some RANS solutions that agreed very well with the high-lift data. With only one exception[c], these were results that used the SA turbulence model. If one selects the entries that agreed well with C_L at $\alpha = 19.57°$

[c]The one RANS turbulence model other than SA that achieved reasonable levels of lift near $C_{L,max}$ was the Menter shear stress transport (SST) model, with its a_1 parameter increased from 0.31 to 1.0. The only other non-SA model used in HLPW-4/GMGW-3 was a k-ϵ lag-based model, but it yielded lower levels of lift near $C_{L,max}$.

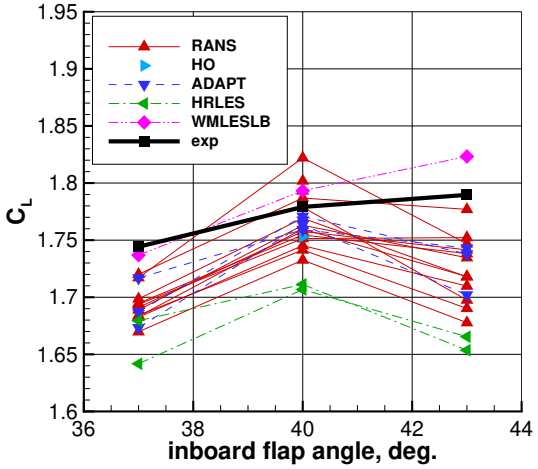

(a) Lift coefficient, BP results

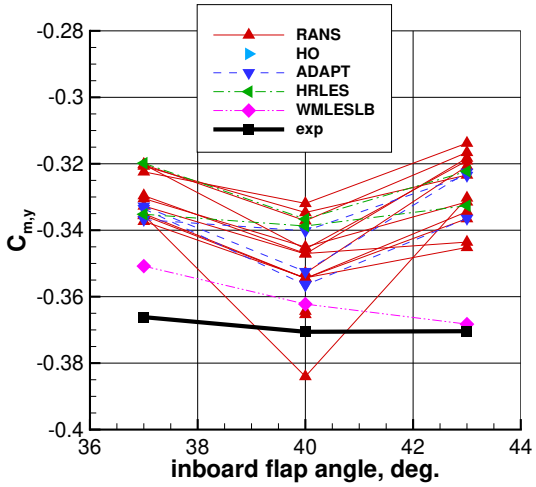

(b) Pitching moment coefficient, BP results

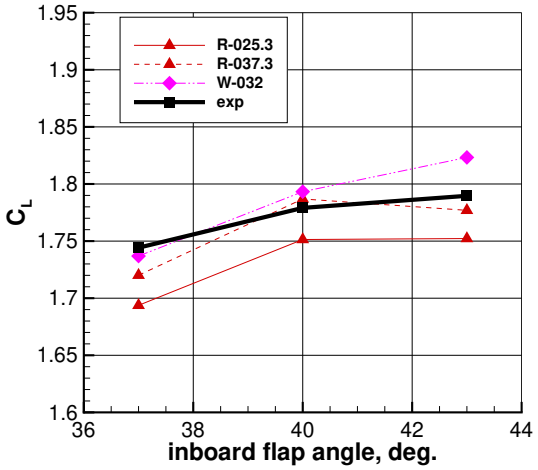

(c) Lift coefficient, selected results

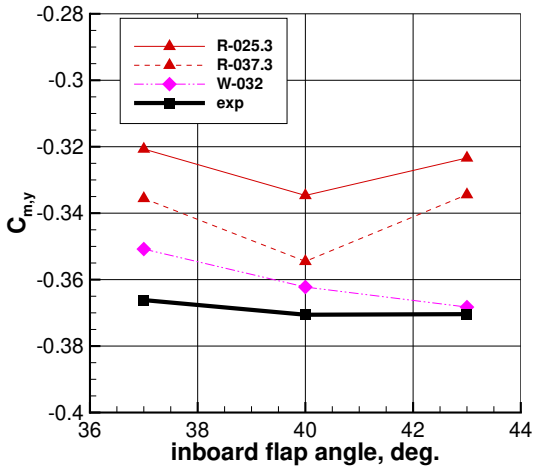

(d) Pitching moment coefficient, selected results

Figure 7. Predictions of flap deflection effects.

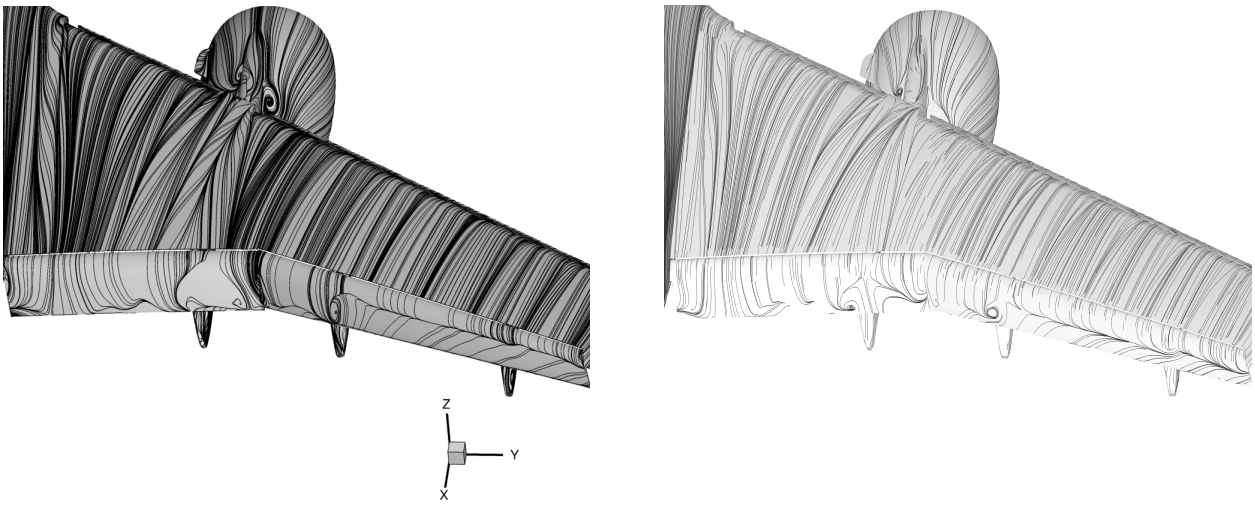

(a) CFD results from R-025.3

(b) CFD results from W-032

(c) Oil flow on wind tunnel model

Figure 8. CRM-HL surface streamlines, $\alpha = 7.05^\circ$ (uncorrected $\alpha_u = 5.98^\circ$), nominal flap angle.

and then looks at surface streamline and skin friction contour patterns, a general trend emerges. The oil flow pattern outboard on the main wing at this angle of attack is shown in Fig. 10(a); there are several wedges of separated flow that start beyond midchord of the main element, apparently influenced by the wakes of several of the slat brackets. Most of the RANS results with reasonable C_L predictions exhibited excessive separation in this region. An example is shown in Fig. 10(b), which shows surface skin friction from one of the ADAPT solutions, A-025.1 (SA model). This same separation pattern was seen consistently among the ADAPT results. This particular solution yielded $C_L = 2.53$, very close to the experimental value of about 2.52 at the same corrected angle of attack. With excessive separation occurring outboard, this RANS solution is somehow compensating for the loss in outboard lift with excessive lift elsewhere, ending up with a fortuitously good prediction of C_L.

On the other hand, a typical HRLES solution (L-016.7, with $C_L = 2.53$) shown in Fig. 10(c), and a typical WMLES solution (W-020.3, with $C_L = 2.54$) shown in Fig. 10(d) indicate better correlation with experimental flow separation patterns. Thus, it appears that near $C_{L,max}$, the scale-resolving CFD simulations generally capture the outboard separated flow physics better than RANS, while also capturing the correct level of vehicle lift. This trend was also noted from the Lattice-Boltzmann solutions at HLPW-3 [5]. This is not to say that the scale-resolving simulations are perfect. As will be described below, considering the goal of accuracy and consistency in high-lift predictions, there is still work to be done to bring these methods to maturity.

It is important to emphasize that the mesh can have a major effect on separation aspects of the solutions, even on those mesh levels that may be considered resolved enough to be "best practice" (BP). For example, using SA RANS, R-025.3 (388 million nodes) was considered to be BP. It produced outboard flow separation patterns that showed similar qualitative trends relative to the oil flow at $\alpha = 19.57^\circ$ ($C_L = 2.56$), but then in R-025.4 on a finer mesh (550 million nodes) the outboard separation pattern was massive ($C_L = 2.51$), like other participants' SA RANS solutions (see Kiris et al. [16]).

Although not covered here, it is worth noting that the upper nacelle lip was a problematic area for many computations at high angles of attack, where separation occurred for some participants but not for others (separation did not occur in the experiment, with the nacelle tripped). The current nacelle design is believed to be very close to separation at high angles of attack; it has been redesigned for future official versions of the CRM-HL.

D. Statistical Analysis

A statistical analysis was performed on the HLPW-4/GMGW-3 data from Test Case 2a (free-air computations) at two representative angles of attack: $\alpha = 7.05^\circ$, representing the linear portion of the lift curve, and $\alpha = 19.57^\circ$, representing maximum lift. This type of analysis has been performed for all previous HLPWs as well. It provides a feel for the trends in the data, including its median and scatter. The scatter is defined as $2K\hat{\sigma}$, where $\hat{\sigma}$ is the standard deviation of the data, and K is a confidence interval coverage factor, taken to be $\sqrt{3}$. This statistical analysis allows us to assess how consistent or inconsistent the CFD is. Here, we segregate the data by TFG, looking only at BP results. Note that there were only two HO results, so its scatter is not meaningful.

In Fig. 11, C_L results from all BP submissions at the two angles of attack are shown. Figures 11(a) and (c) show individual results grouped according to TFG. (Recall that the WMLESLB results included three different methods besides the majority WMLES submissions: one was a high-order WMLES result, one a Lattice-Boltzmann result, and one an Euler result. Because these three are unique, they are pointed out in the figure. However, they did not skew the WMLESLB statistics much.) For reference, the measured experimental result is included as a thick black dash-dot line. The individual participant BP results are given as symbols, with a different color and symbol type for each TFG. The median for each TFG is given as a horizontal colored line. At $\alpha = 7.05^\circ$ (Fig. 11(a)), the median result from RANS and ADAPT were closest to the corrected experimental result. The HO and HRLES results were too low by roughly $\Delta C_L = 0.05 - 0.07$, and the WMLESLB results were too high by about $\Delta C_L = 0.04$. In terms of scatter for $\alpha = 7.05^\circ$, shown in Fig. 11(b), the RANS, HRLES, and WMLESLB were very similar (near 0.1), whereas the ADAPT scatter was notably smaller.

Figure 11(c) shows C_L at $\alpha = 19.57^\circ$. The HRLES and ADAPT median values came closest to the corrected data, with WMLESLB also fairly close. The RANS median was low by about $\Delta C_L = 0.15$. HO results were much lower, but there were only two entries. Also note that HRLES had only three BP results for this angle of attack. The RANS scatter shown in Fig. 11(d) was very high, near 0.68, reflecting the large variation in results. However, the specific RANS-based solutions that used adaptive meshing (ADAPT) yielded much lower scatter near 0.15. The scatter in HRLES and WMLESLB at $\alpha = 19.57^\circ$ was also similarly low.

From HLPW-3 on a different high-lift configuration, the $2K\hat{\sigma}$ scatter was around $\Delta C_L = 0.15$ in the linear part of the lift curve, and near 0.6 near $C_{L,max}$. Thus, in HLPW-4/GMGW-3 the RANS scatter at low angle of attack was reduced somewhat compared to HLPW-3, but the scatter did not improve at all (in fact, it got slightly worse) near

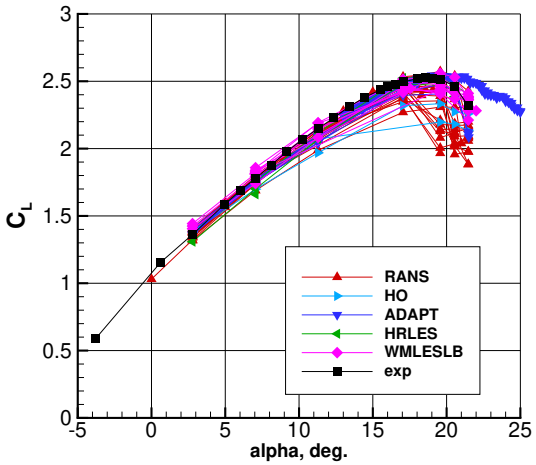

(a) Lift coefficient, free air, corrected α

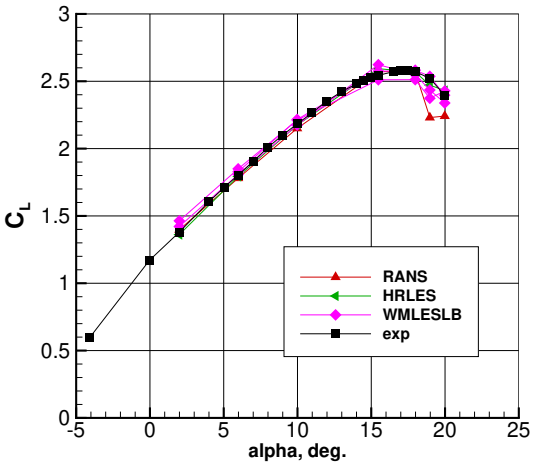

(b) Lift coefficient, in tunnel, uncorrected α

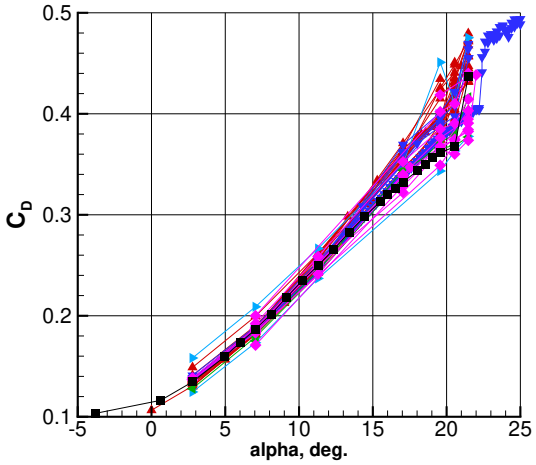

(c) Drag coefficient, free air, corrected α

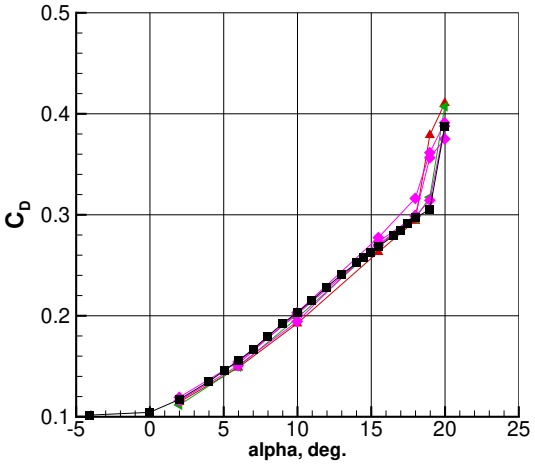

(d) Drag coefficient, in tunnel, uncorrected α

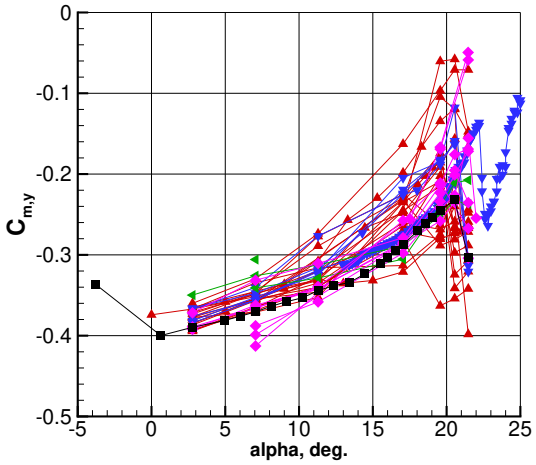

(e) Pitching moment coefficient, free air, corrected α

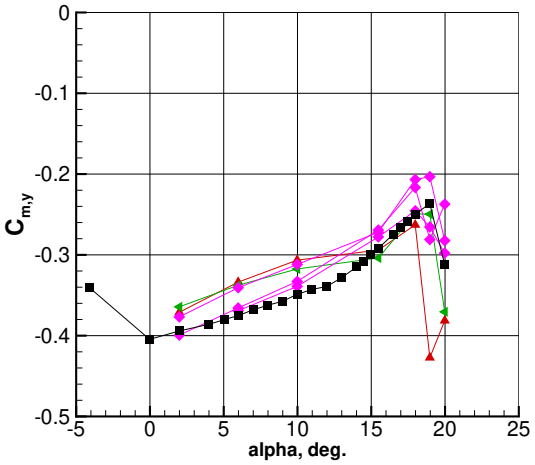

(f) Pitching moment coefficient, in tunnel, uncorrected α

Figure 9. CRM-HL force and moment comparisons (BP results), nominal flap angle.

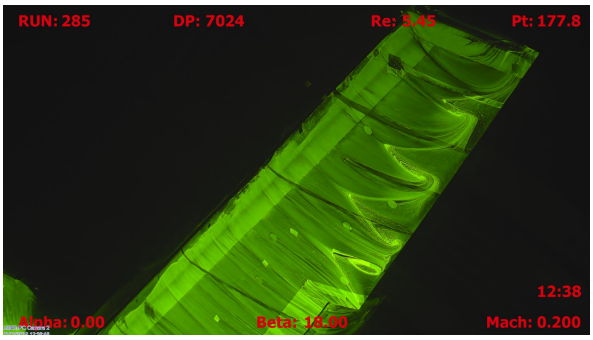

(a) Oil flow at $\alpha_u = 17.98°$

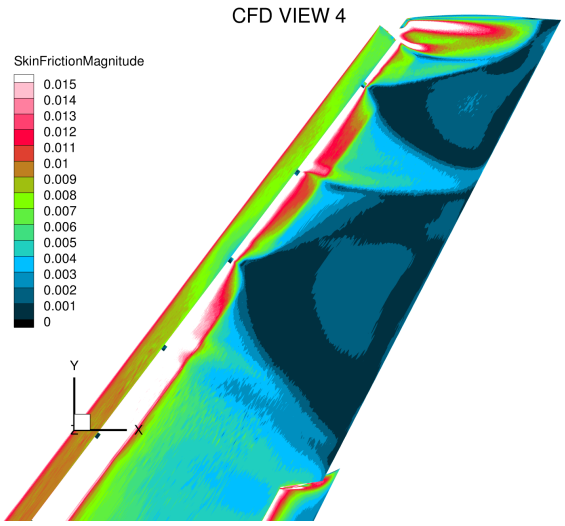

(b) C_f contours from A-025.1 (RANS with SA model)

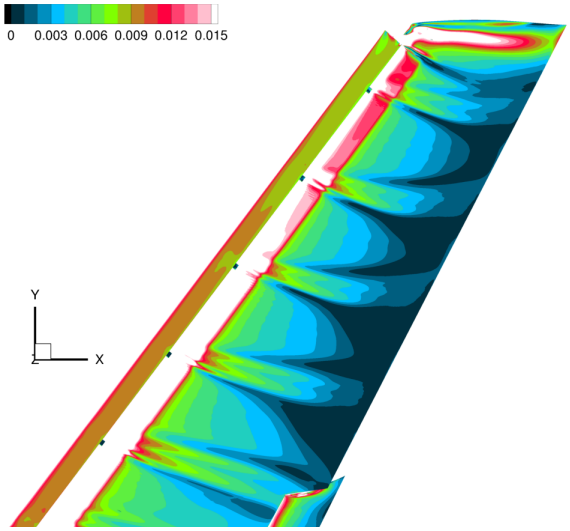

(c) C_f contours from L-016.7 (HRLES)

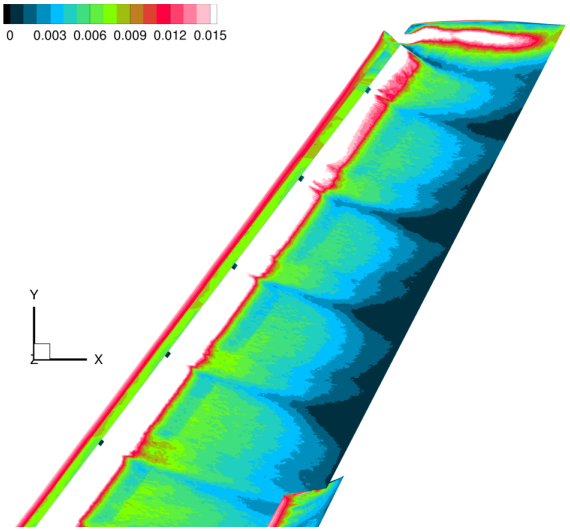

(d) C_f contours from W-020.3 (WMLES)

Figure 10. CRM-HL oil flow and surface skin friction contours from free-air computations at $\alpha = 19.57°$, nominal flap angle.

$C_{L,max}$. Although not shown, C_D and $C_{m,y}$ were also analyzed in this same statistical way. RANS scatter levels were similar to those from HLPW-3, and ADAPT scatter levels were again much lower.

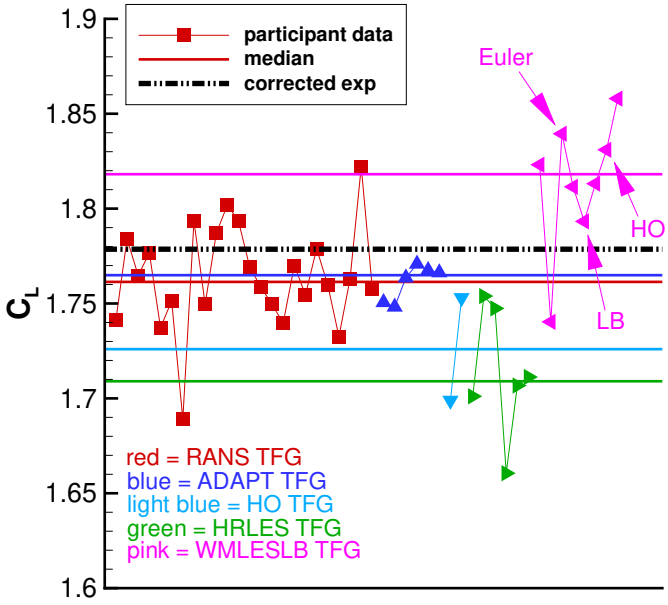

(a) Results at $\alpha = 7.05°$

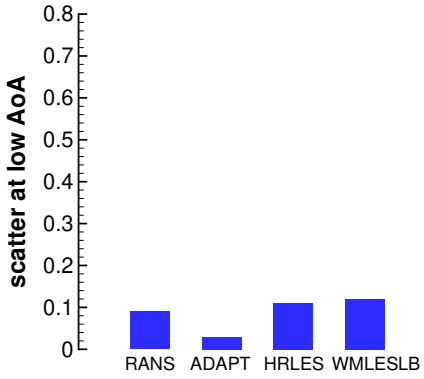

(b) Scatter at $\alpha = 7.05°$

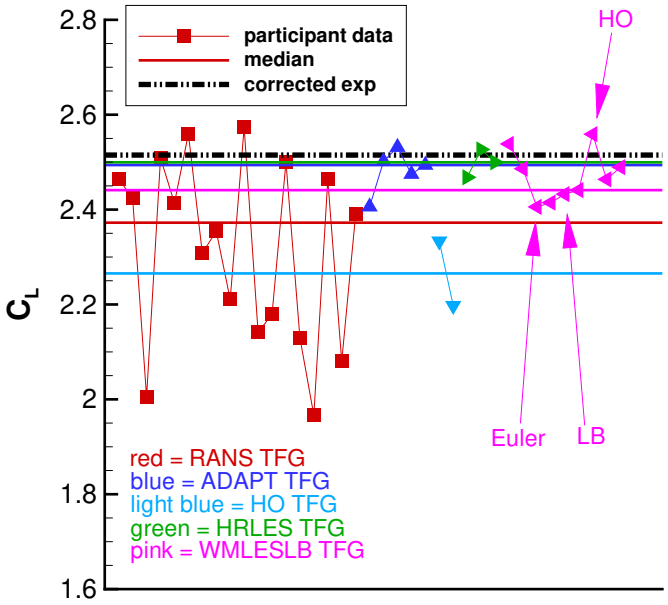

(c) Results at $\alpha = 19.57°$

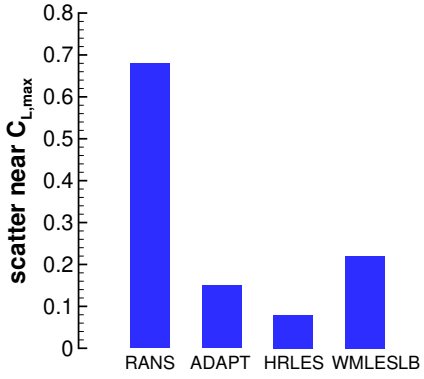

(d) Scatter at $\alpha = 19.57°$

Figure 11. Statistical analysis of free-air C_L predictions, BP results.

E. Other Analysis

A very brief summary of other analysis of the submitted data is provided in this section.

1. *Iterative Convergence*

Iterative convergence of RANS-based submissions (RANS, HO, and ADAPT) is examined in this section for two angles of attack of $\alpha = 7.05°$ and $\alpha = 19.57°$. Results (BP only) are shown in Fig. 12. The iterative history provided by each participant was scaled to lie between 0 and 1 (0 indicating the start of recorded data, 1 indicating the end of recorded data). Some participants did not submit iterative histories.

Figure 12(a) shows results at $\alpha = 7.05°$. Out of 22 results, 3 showed significant slope or variation even near the end of their run, suggesting a lack of sufficient iterative convergence. These are indicated in the figure with black arrows. There were 12 results that appeared to converge to a relatively steady solution, and 7 results that were unsteady but with a fairly flat mean (with either low-frequency or high-frequency oscillations).

The results in Fig. 12(b) at $\alpha = 19.57°$ show that out of 17 solutions, 3 appeared to have insufficient iterative convergence (indicated by black arrows), 8 were flat (converged to a steady state), and 6 oscillated around some mean.

These results highlight the difficulty often associated with obtaining converged RANS solutions for complex configurations like the CRM-HL. If iterative convergence is not fully achieved, then there is some uncertainty associated with that solution. As a result, it is possible that some of the differences between CFD results may be from lack of iterative convergence.

Although not covered here, sufficient convergence of scale-resolving simulations is also important. In this case, convergence means something different than for steady-state RANS: after the simulation has been run long enough to rid itself of nonphysical transients, it must be run further and long-time-averaged over a sufficient interval of time so that an adequately-converged steady-state mean solution is achieved. It can be difficult to ascertain success, because the mean can sometimes appear (by eye) to be converged, but additional iterations can sometimes yield further changes. Also, some quantities of interest (lift, pressures) typically converge faster to a long-time mean that others (velocity, Reynolds stresses). The HRLES [12] and WMLESLB [13] summary papers discuss temporal averaging for scale-resolving simulations further.

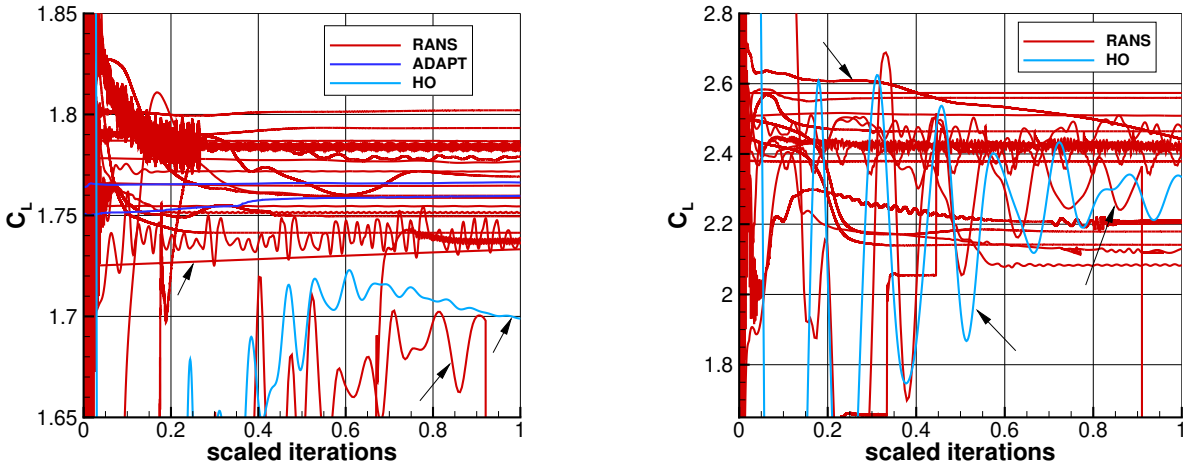

(a) Results at $\alpha = 7.05°$

(b) Results at $\alpha = 19.57°$

Figure 12. Scaled iterative convergence of C_L for RANS-based methods, BP results.

2. *Velocity Profiles*

HLPW-4/GMGW-3 participants were asked to submit velocity profiles at 15 different locations over the CRM-HL upper surface, even though there are not yet any measured flowfield data over this configuration. These velocity profiles help to provide another measure of the CFD consistency (or lack thereof). A sample of results is shown in Fig. 13 for $\alpha = 7.05°$ and Fig. 14 for $\alpha = 19.57°$. Figures 13(a) and 14(a) show the locations where velocity data

were collected, with pink arrows denoting the locations shown in each figure. The locations were divided into 4 groups (A, B, C, and D) out the span of the wing.

For $\alpha = 7.05^\circ$ in Fig. 13, u velocity profiles at location A.1 indicate excellent agreement between most CFD results. The only exceptions were the two HO results and W-047, which combined HO with WMLES. At location B.4, there was no clear trend among the RANS results; all were separated. HRLES and WMLESLB were less separated. At location C.1, most of the RANS, ADAPT, and WMLESLB were very similar to each other. Again the HO results (including W-047) stood out. The HRLES results were similar to each other, with greater edge velocity and deeper slat-wake deficit than most of the other profiles.

For $\alpha = 19.57^\circ$ in Fig. 14, the profiles (shown at different locations from Fig. 13) indicate a very wide range of predicted solutions, even considering a given TFG category. (The two ADAPT solutions look very similar to each other, but they were both from the same participant; they employed different types of error indicators for mesh adaptation.) Note that most of the results at locations A.4 and D.1 are indicating attached flow, yet there was still a significant spread in the results at these locations.

It is important to note that an analysis taking into account the particular meshes employed was not performed. Based on past experience [4], the mesh resolution locally can have a significant influence on computed profiles, including in wake regions away from the wing surface where mesh points are not typically clustered. In any case, the velocity profiles shown here demonstrate how different codes' results can yield consistent velocity profiles in some regions, but very inconsistent profiles in others, particularly in separated areas and near $C_{L,max}$. It is hoped that some of the future high-lift ecosystem wind tunnel testing can acquire boundary layer profile validation data, which will help determine which models and methods are most accurate.

VI. Workshop Key Questions and Status

In this section, we address the six high-level Key Questions from HLPW-4/GMGW-3, and – based on what was learned at the workshop – provide the current status of the answers to them.

A. KQ #1

What CFD solution methodology(ies) currently provides the best/most-consistent approach to predicting (a) increments due to flap deflection, and (b) maximum lift?

The answers to this KQ were gleaned both from the individual TFG studies as well as from the workshop results as a whole, shown in this paper.

For predicting increments due to flap deflection (when the flap includes separated flow), the RANS-based methods were unsuccessful as well as inconsistent. There was one result from a Lattice-Boltzmann method that indicated a favorable trend, but two HRLES submissions did not predict the trends well. Therefore, more studies are needed using scale-resolving methods to determine their efficacy.

For predicting $C_{L,max}$, the scale-resolving methods used in the HRLES and WMLESLB TFGs showed better correlation with test data than RANS, both with respect to capturing separated flow physics and achieving the right answer for the right reasons outboard on the wing. Near the wing root, there are currently too many unresolved questions regarding the influence of the tunnel floor boundary layer on the semispan model to draw any firm conclusions. In spite of the better success of scale-resolving simulations near $C_{L,max}$, consistency in those results as a whole was still lacking. Much of this inconsistency may be due to the effects of mesh resolution. Firmer best-practice guidelines are still needed for achieving adequate meshing for high-lift flows over complex configurations when using HRLES and WMLES.

B. KQ #2

What are important lessons learned in high-lift CFD analysis explored in HLPW-4?

Besides the conclusions reached for KQ #1, other lessons have emerged from the separate TFG studies that were presented at the workshop. They are covered in more detail in other summary papers [9–13]. However, for completeness, a few lessons learned are briefly mentioned here.

For fixed-grid RANS, adequate mesh convergence was generally not achieved. The finer "D-level" committee-generated meshes with greater than 200 million mesh nodes appeared to be sufficiently fine only in the linear range of the lift curve, away from stall. Near stall, no conclusions regarding mesh suitability, even on the finest meshes,

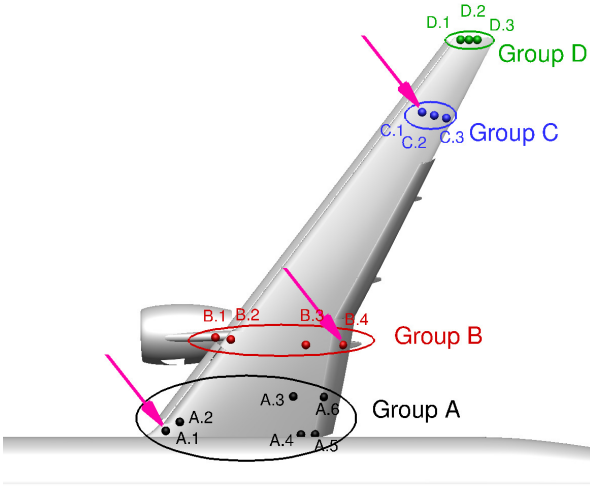

(a) Locations of profiles

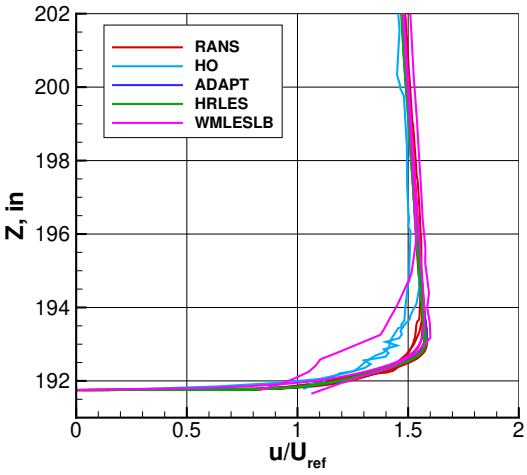

(b) Profile A.1

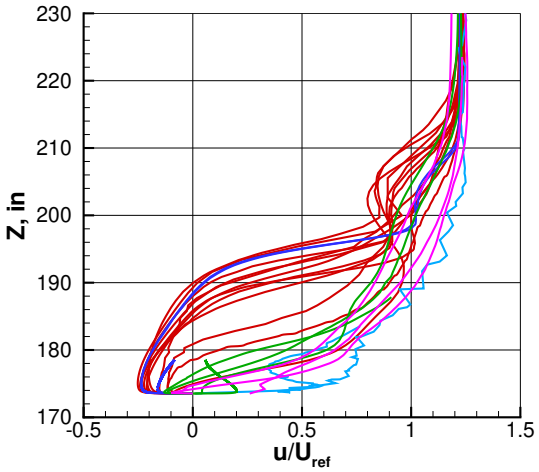

(c) Profile B.4

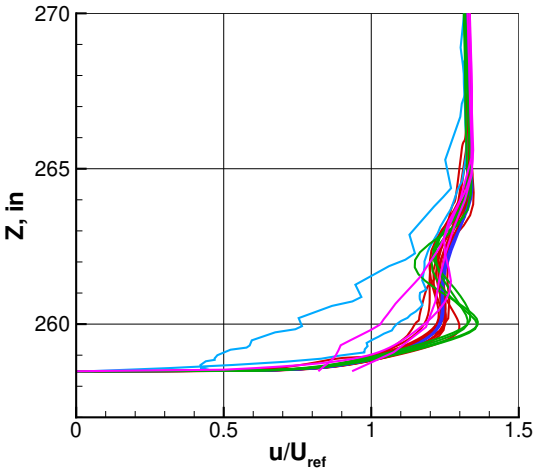

(d) Profile C.1

Figure 13. u **velocity profiles over the CRM-HL upper surface,** $\alpha = 7.05°$**, BP results.**

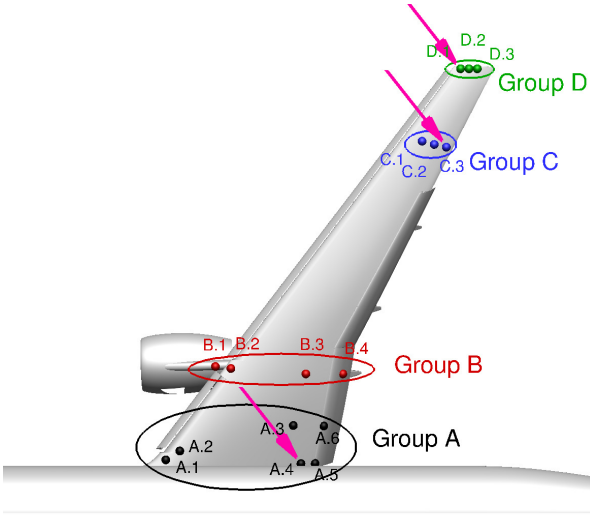

(a) Locations of profiles

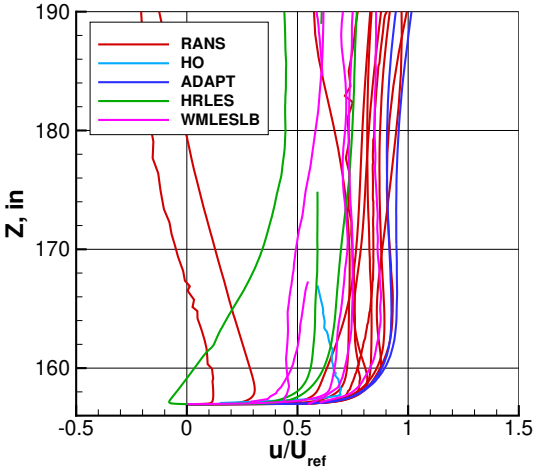

(b) Profile A.4

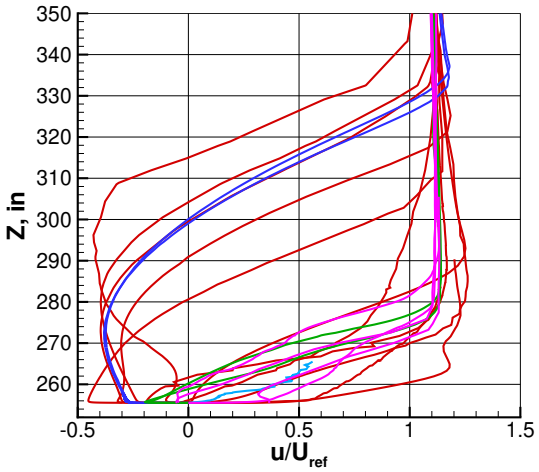

(c) Profile C.3

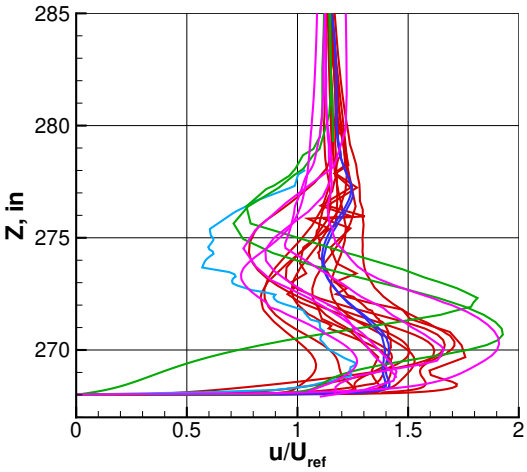

(d) Profile D.1

Figure 14. u **velocity profiles over the CRM-HL upper surface,** $\alpha = 19.57°$**, BP results.**

were possible. Many codes lacked the ability to achieve deep (machine zero) iterative convergence for the CRM-HL configuration, and it was not possible to determine how much error came from this source.

For HO, the best-practice meshing guidelines were quite different than for RANS. Mesh curving in three dimensions for highly anisotropic elements was a formidable task. Implicit solvers were found to be critical for solving high-order discretizations. Overall, applying high-order finite-element and finite-volume methods to the CRM-HL configuration was demonstrated, but was very challenging.

In the RANS-based ADAPT solutions, regions of suspected multiple solutions were made more consistent with mesh refinement and better iterative convergence. It was also demonstrated that mesh adaptation can automatically track and resolve vortices and wakes in the CRM-HL flowfield. The multiscale metric was slower to propagate features such as slat wakes than goal-based methods.

For HRLES, mesh designs that led to RANS mesh convergence did not lead to HRLES mesh convergence, and mesh resolution was seen to have a big impact on predicted separation patterns. A typical HRLES run was approximately 10 to 15 times more costly than RANS. In some explorations with wind-tunnel runs, it was difficult to match the shape and thickness of the measured tunnel wall boundary layer, and this was found to have an impact on the solution. In terms of averaging time, approximately 40 convective time units (CTUs) (the time it takes for a particle in the freestream to travel the length of the mean aerodynamic chord) was found to be sufficient for most of the angles of attack; higher angles near and beyond stall required more CTUs than lower angles. Finally, both cold starts (starting the CFD run from freestream conditions) and warm starts (restarting from a previous HRLES solution at a different angle of attack) were found to be superior than restarting from a RANS solution at the same angle of attack. In the latter case, the HRLES solution seemed to "inherit" and preserve any massive separation characteristics from the RANS solution.

For WMLESLB, a large sensitivity to mesh resolution and mesh characteristics such as cell anisotropy was found at and beyond stall. Like with HRLES, mesh resolution was seen to have a big impact on predicted separation patterns. A typical WMLES run was approximately 5 to 10 times more costly than RANS. For half-model testing, further investigations are needed to understand the competing roles of the tunnel boundary layer, standoff height, and tunnel blockage. Numerical tripping was found to be more cost effective than attempting to represent the actual tripping mechanism from the wind tunnel test. In terms of averaging time, high angles of attack required longer than low angles to make sure that stationarity was achieved.

C. KQ #3

What geometry and meshing best practices are appropriate for high-lift CFD analysis for RANS, Wall Modeled LES, and Hybrid RANS/LES simulations?

Data were collected and analyzed from the TFG summary presentations, the GEOM TFG geometry and meshing challenges, and participant questionnaires completed by committee members and participants who created meshes to see if new or modified best practices could be identified in geometry preparation or mesh generation techniques. Limited participation in the geometry and meshing challenges made it difficult to draw concrete conclusions on best practices. However, there were high-level observations made that will be discussed here, which merit further investigation in future studies and workshops.

Multiple participants and TFG members noted that the development of guidelines for geometry modeling and modification operations could significantly reduce downstream time spent in the mesh generation process. Creating a suitable surface mesh for the CRM-HL typically involved an initial step with some level of automation to get a surface mesh followed by manual intervention at various locations to deal with regions in the geometry where additional surface trimming, topological splits, or other forms of model modification were required. It is important to note that these modifications were not necessarily to correct issues within the geometry but to make it more suitable for the needs of current CFD meshing software. For example, in the provided CRM-HL CAD files, the geometry model did not have a defined boundary edge along the leading edge of the wing. Multiple participants chose to split the CAD topology along the leading edge of the wing to create a boundary edge with which their mesh generation software could provide alignment, sizing, and/or post-processing control. Because there is no guideline for where or how these topological splits were made, there was variability in the split location from participant to participant. It is unknown at this time whether this variability could have downstream impact on the final volume meshes and subsequent solutions. Further investigation is warranted to understand whether there could be any mesh effect on the simulation from the location of this split and, if so, what would be the best practice recommendation for the optimum location. There were other discussions surrounding the trimming locations of the Wing Under Slat Surface (WUSS) with the upper wing

surface, on reducing problematic pinch points in adjacent surfaces, and on the issue of gaps in the model being larger than meshing guidelines for minimum spacing.

There was a preference among some observers and participants for the use of solid model geometry or parametric representations instead of the piecemeal surface representations used within the workshop. Within their typical meshing workflows these types of geometry models enabled easier geometry assembly and modification. Additionally, the concept of using surrogate/virtual geometries for complex geometries came into play within the mesh adaption and high-order discretization TFGs and may enable greater success with those methodologies.

As expected, mesh design and requirements varied significantly between fixed-grid RANS, HRLES, WMLES, and HO. For instance, the meshing guidelines that led to fixed-grid RANS convergence did not lead to HRLES mesh convergence. Within HRLES, it was observed that increased mesh resolution in the separated-flow regions appeared to significantly improve HRLES predictions whereas a similar treatment did not yield the same results for RANS simulations. Within the WMLESLB TFG, it was noted that there was significant sensitivity to streamwise mesh spacing, particularly in the outboard section of the wing where there was large geometric curvature, when reviewing the sensitivity of the integrated pitching moment coefficient at both the lowest and highest angles of attack.

D. KQ #4

What roadblocks in geometry preparation and mesh generation for CFD prevent analysts from creating geometry/meshes suitable for high-lift aerodynamics simulations in a turn-key, rapid manner?

Using the same sources as KQ #3, some high-level answers to this KQ follow. The current lack of understanding with regard to how geometry preparation choices impact meshing and simulations in complex regions is a roadblock to developing appropriate CFD-related geometry modeling best practices. In turn, the lack of consistent best practices for the build-up and modification of complex geometric regions can be considered a primary driver in the need for manual intervention in geometry preparation and mesh generation processes. Additional studies are warranted in these areas to help the community decrease the turn-around time in both geometry preparation and mesh generation for high-lift configurations.

Remaining hindrances to seeing geometry and mesh generation become more turn-key revolve around computational resources. There was a desire in this workshop to broadly explore mesh resolution for RANS mesh convergence studies by using finer mesh levels than past workshops and to expand beyond RANS to scale-resolving methods. While current mesh generators have demonstrated the ability to generate CRM-HL meshes in excess of 1 billion cells [7], many participants encountered difficulty running meshes of this size or even smaller. Participants often lacked access to a computational resource large enough to run the largest mesh sizes. Those researchers with access to a large enough resource often lacked sufficient time on it to explore simulations extensively. A final and recurring problem within the workshop framework was also the ability to exchange large mesh files easily and quickly between members of the community.

As discussed in KQs #2 and #3, a better understanding is needed of the differences in meshing requirements for RANS, HRLES, WMLES, LB, and high order simulations in different regions of the lift curve.

E. KQ #5

What was the impact/effectiveness of the existing test data collected for the CRM-HL configuration in understanding high-lift flow physics? If not effective, what is needed?

The following test data proved to be (at least partially) effective for HLPW-4/GMGW-3. Corroborating data sources (force and moment measurements, surface pressures, minitufts, and oil flow) used for the primary test cases helped to determine if a simulation achieved the "right answer for the right reasons." A definition of the wind-tunnel contraction and diffuser sections, updated test section geometry, and run procedures for mimicking the wind tunnel test data acquisition provided valuable insights and raised new questions about in-tunnel CFD runs.

Some problematic areas included not knowing the full characterization of tunnel inflow conditions and wall/floor boundary layer development. This hampered efforts to fully understand differences seen between test data and in-tunnel CFD simulations, particularly near $C_{L,max}$. The lack of off-body boundary layer and wake data over the CRM-HL hampered efforts to understand details of the stall mechanism at $C_{L,max}$, especially in the slat wakes, near and downstream of the nacelle/pylon intersection with the wing, and near the wing-body juncture. Detailed boundary layer profiles at key locations such as these would help to further assess and improve CFD.

F. KQ #6

What are the significant remaining technical areas that require additional focus in future workshops?

Workshop participants responded to this KQ as part of a questionnaire; a few of the responses are mentioned here. For fixed-grid technology, a focus on the fidelity of the mesh needed near $C_{L,max}$ (for both RANS and scale-resolving methodologies) is required. Additional focus on high-order and curved meshing would be helpful to the HO community. There is a desire to expand mesh adaptation to eddy-resolving methods. In terms of flow solver technology, there needs to be a continued focus on verification, reproducibility, and consistency. Methods for verification need to be found for scale-resolving simulations. Common simple unit test problems between RANS and scale-resolving simulations may be helpful. Other studies should include hysteresis and solution path dependency, turbulence model studies, and wall function studies. Measurements of specific wind tunnel boundary conditions and flowfield data were also noted, but most of these were covered in KQ #5.

VII. Conclusions

HLPW-4/GMGW-3 broke new ground with its use of Technology Focus Groups (TFGs) that met regularly for well over a year prior to the workshop. The TFGs encouraged greater collaboration among participants, so that more rapid progress could be made toward the ultimate goal of achieving reliable predictions of high-lift flows. HLPW-4/GMGW-3 also collected far more data than any of the previous workshops. Much of it remains to be analyzed.

The joint workshop model between HLPW-4 and GMGW-3 enabled a greater focus on meshing, which continues to have a very large influence on the CFD solutions. Geometry preparation and fixed-grid meshing for high-lift flows is still difficult. It is not clear how to best handle complex regions like junctions and pinch points. It is also very difficult to determine fixed-grid guidelines for different methodologies, codes, and regions of the lift curve. Perhaps if there was enough compute power and code capability to regularly run CFD on meshes with tens or hundreds of billions of unknowns, the influence of the mesh could be effectively diminished for realistic problems near maximum lift. But many groups are limited to routine use of meshes with no more than a few hundred million unknowns, so mesh influence is still quite dominant. Mesh adaptation represents a possible solution to this issue, but most CFD codes still do not possess this capability.

Verification continues to figure prominently in the HLPWs. In this workshop, a 2-D multielement airfoil verification case using the Spalart-Allmaras turbulence model yielded generally good results for almost all participants that provided data for it. This represents a dramatic improvement from HLPW-3, when only 30% of the participants passed the verification exercise. Having verified CFD codes helped to narrow down the cause of solution differences to (primarily) discretization and iterative convergence errors. The latter issue continues to be problematic because most CFD codes cannot fully converge to a steady state (with residuals near machine zero) on complex cases like the CRM-HL.

For high-lift flows, RANS was still incapable of predicting the forces and pitching moment accurately and consistently. And even for the few cases when lift was predicted correctly, it could be shown to be for the wrong reasons: RANS tended to predict much more outboard separation than the wind tunnel test article near $C_{L,max}$. In fact, RANS also failed to predict flap deflection effects at low angle of attack away from stall. However, both situations involved significant regions of separated flow, which is the Achilles heel of RANS.

High-order methodologies were still an emerging technology for complex geometries like the CRM-HL. Although they performed very well for the 2-D verification exercise, the high-order CRM-HL results did not fare as well compared to other methods. Nonetheless, much progress was made with respect to high-order meshing and high-order algorithms, and their promise of higher accuracy at lower cost is an enticing goal that would help overcome many barriers.

Mesh adaptation technology brought much more consistency to the high-lift results. Adapted results for the SA turbulence model were typically very close to each other in terms of surface flow topology. Because they were RANS-based, the adapted results were still deficient compared to the experimentally-measured data near $C_{L,max}$, but they were far more *consistent* than the fixed-grid RANS results. Consistency is crucial for drawing firm conclusions in validation efforts.

Scale-resolving simulation methods appeared to be most promising for predicting $C_{L,max}$. On the outboard part of the wing, they produced less separation than RANS, in better agreement with the measured oil flow data. (Inboard near the wing root, there is still some question as to the influence of the tunnel floor boundary layer near maximum lift conditions; so it is not yet clear what the correct flow pattern should be there when running in free air.) However, there

were still notable inconsistencies among the scale-resolving results, particularly in velocity profiles. And at low angles of attack, the scale-resolving methods appeared to be somewhat *less* accurate than RANS. Therefore, more work is needed to mature these approaches and establish best practice guidelines.

Finally, additional measured data are needed for further validation of the CFD. Off-body boundary layer velocity and Reynolds stress profiles, as well as measurements of off-body vortical structures, would be invaluable for future validation activities. While most HLPW-4/GMGW-3 participants only ran free-air computations, future validation efforts will likely involve more in-tunnel runs. For those, it will be helpful to have as complete a wind-tunnel characterization as possible, including upstream tunnel wall boundary layer profiles and inflow stream uniformity maps.

Acknowledgments

The authors gratefully acknowledge Amazon Web Services for providing access to sufficient computing storage to house HLPW-4/GMGW-3 meshes and datasets, and to Tecplot Inc. for providing temporary licenses to workshop participants for use in postprocessing their CFD results. The organizing committee would like to thank all of the participants for their efforts during the course of the workshop activity, and especially the TFG leaders who tirelessly organized and facilitated regular meetings to share results so that technical efforts could be better directed to achieve TFG and workshop goals. The first author also acknowledges the NASA Transformational Tools and Technologies (TTT) project of the Transformative Aeronautics Concepts Program, which strongly supports the HLPW series.

References

[1]Rumsey, C. L., "The 4th AIAA CFD High Lift Prediction Workshop (HLPW-4)," https://hiliftpw.larc.nasa.gov, Accessed: 2022-03-28.

[2]Woeber, C., "3rd AIAA Geometry and Mesh Generation Workshop," https://www.gmgworkshop.com, Accessed: 2022-03-28.

[3]Rumsey, C. L., Slotnick, J. P., Long, M., Stuever, R. A., and Wayman, T. R., "Summary of the First AIAA CFD High-Lift Prediction Workshop," *Journal of Aircraft*, Vol. 48, No. 6, 2011, pp. 2068–2079, doi: https://doi.org/10.2514/1.C031447.

[4]Rumsey, C. L. and Slotnick, J. P., "Overview and Summary of the Second AIAA High-Lift Prediction Workshop," *Journal of Aircraft*, Vol. 52, No. 4, 2015, pp. 1006–1025, doi: https://doi.org/10.2514/1.C032864.

[5]Rumsey, C. L., Slotnick, J. P., and Sclafani, A. J., "Overview and Summary of the Third AIAA High Lift Prediction Workshop," *Journal of Aircraft*, Vol. 56, No. 2, 2019, pp. 621–644, doi: https://doi.org/10.2514/1.C034940.

[6]Chawner, J. R., Michal, T., Slotnick, J. P., and Rumsey, C. L., "Summary of the 1st AIAA Geometry and Mesh Generation Workshop (GMGW-1) and Future Plans," AIAA Paper 2018-0128, January 2018, doi: https://doi.org/10.2514/6.2018-0128.

[7]Woeber, C. D., Masters, J. S., and McDaniel, D. R., "Summary of Exascale and Remeshing Efforts for the Second Geometry and Mesh Generation Workshop," AIAA Paper 2019-3458, June 2019, doi: https://doi.org/10.2514/6.2019-3458.

[8]Spalart, P. R. and Allmaras, S. R., "A One-Equation Turbulence Model for Aerodynamic Flows," *Recherche Aerospatiale*, No. 1, 1994, pp. 5–21.

[9]Ollivier-Gooch, C. F. and Coder, J. G., "Lessons Learned by the Fixed-Grid RANS TFG for HLPW-4 / GMGW-3," AIAA Aviation paper to appear, 2022.

[10]Galbraith, M. C. and Karman, S. L., "HLPW-4/GMGW-3: High Order Discretization Technology Focus Group Workshop Summary," AIAA Aviation paper to appear, 2022.

[11]Park, M., Alauzet, F., and Michal, T., "HLPW-4/GMGW-3: Mesh Adaptation for RANS Technology Focus Group Workshop Summary," AIAA Aviation paper to appear, 2022.

[12]Ashton, N., Batten, P., Cary, A. W., Holst, K. R., and Skaperdas, V., "HLPW-4/GMGW-3: Hybrid RANS/LES Technology Focus Group Workshop Summary," AIAA Aviation paper to appear, 2022.

[13]Kiris, C., Ghate, A., and Browne, O., "HLPW-4/GMGW-3: Wall-Modeled LES and Lattice-Boltzmann Technology Focus Group Workshop Summary," AIAA Aviation paper to appear, 2022.

[14]Pita, C. and Woeber, C., "HLPW4/GMGW3: Summary of Fixed Mesh Generation Efforts for RANS Analyses," AIAA Aviation paper to appear, 2022.

[15]Duensing, J. C., Housman, J. A., Fernandes, L. S., Machado, L. G., and Kiris, C. C., "A Reynolds-Averaged Navier-Stokes Perspective for the High Lift-Common Research Model Using the LAVA Framework," AIAA Aviation paper to appear, 2022.

[16]Kiris, C. C., Ghate, A. S., Duensing, J. C., Browne, O. M. F., Housman, J. A., Stich, G.-D., Kenway, G. K., Fernandes, L. S., and Machado, L. G., "High-Lift Common Research Model: RANS, HRLES, and WMLES Perspectives for CLmax Prediction using LAVA," AIAA Paper 2022-1554, January 2022, doi: https://doi.org/10.2514/6.2022-1554.

[17]Wang, L., Anderson, W. K., Nielsen, E. J., Balakumar, P., Park, M. A., Carlson, J.-R., Iyer, P. S., and Diskin, B., "Wall-Modeled Large-Eddy Simulations for High-Lift Configurations using FUN3D," AIAA Paper 2022-1555, January 2022, doi: https://doi.org/10.2514/6.2022-1555.

[18]Goc, K. A., Moin, P., and Bose, S. T., "Large Eddy Simulation of the NASA High-Lift Common Research Model," AIAA Paper 2022-1556, January 2022, doi: https://doi.org/10.2514/6.2022-1556.

[19]Subbian, G., Magrini, A., Benini, E., Buosi, D., Ponza, R., and Radespiel, R., "RANS Analysis of HL-CRM at Landing Configuration with different Flap Deflections and Engine Representations," AIAA Paper 2022-0048, January 2022, doi: https://doi.org/10.2514/6.2022-0048.

[20]Lohry, M. W. and Martinelli, L., "Discontinuous Galerkin Implicit Large Eddy Simulation of Tandem Spheres and the High-Lift Common Research Model," AIAA Paper 2022-1375, January 2022, doi: https://doi.org/10.2514/6.2022-1375.

[21]Balan, A., Wood, S. L., Park, M. A., Anderson, W. K., and Jacobson, K. E., "Angle-of-Attack Sweep with Mesh Adaptation for High-Lift Configurations," AIAA Paper 2022-0218, January 2022, doi: https://doi.org/10.2514/6.2022-0218.

[22]Lacy, D. S. and Clark, A. M., "Definition of Initial Landing and Takeoff Reference Configurations for the High Lift Common Research Model (CRM-HL)," AIAA Paper 2020-2771, June 2020, doi: https://doi.org/10.2514/6.2020-2771.

[23]Lacy, D. S. and Sclafani, A. J., "Development of the High Lift Common Research Model (HL-CRM): A Representative High Lift Configuration for Transonic Transports," AIAA Paper 2016-0308, January 2016, doi: https://doi.org/10.2514/6.2016-0308.

[24]Mauery, T. M., Slotnick, J. P., Cary, A. W., Schaefer, J. A., Lee, V., Malecki, R., Medic, G., Alonso, J. J., and Mavriplis, D., "A 20-year Vision for Flight and Engine Certification by Analysis," AIAA Paper 2022-1553, January 2022, doi: https://doi.org/10.2514/6.2022-1553.

[25]Lin, J. C., Melton, L. P., Hannon, J. A., Andino, M. Y., Koklu, M., Paschall, K. B., and Vatsa, V. N., "Wind Tunnel Testing of Active Flow Control on High-Lift Common Research Model," AIAA Paper 2019-3723, June 2019, doi: https://doi.org/10.2514/6.2019-3723.

[26]Evans, A., Lacy, D., Smith, I., and Rivers, M., "Test Summary of the NASA Semi-Span High-Lift Common Research Model at the QinetiQ 5-Metre Low-Speed Wind Tunnel," AIAA Paper 2020-2770, June 2020, doi: https://doi.org/10.2514/6.2020-2770.

[27]Rumsey, C. L., "The Langley Research Center Turbulence Modeling Resource, VERIF/2DMEA: 2D Multielement Airfoil Verification Case," https://turbmodels.larc.nasa.gov/multielementverif.html, Accessed: 2022-03-28.

[28]Ursachi, C.-I., Galbraith, M. C., Allmaras, S. R., and Darmofal, D. L., "Output-Based Adaptive Reynolds-Averaged Navier-Stokes Higher-Order Finite Element Solutions on a Multi-Element Airfoil," *AIAA Journal*, Vol. 59, No. 7, 2021, pp. 2532–2545, doi: https://doi.org/10.2514/1.J059968.

[29]Michal, T., Krakos, J., Kamenetskiy, D., Galbraith, M., Ursachi, C.-I., Park, M. A., and Anderson, W. K., "Comparing Unstructured Adaptive Mesh Solutions for the High Lift Common Research Model Airfoil," AIAA Paper 2020-3219, June 2020, doi: https://doi.org/10.2514/6.2020-3219.

[30]Rumsey, C. L., "The Langley Research Center Turbulence Modeling Resource," https://turbmodels.larc.nasa.gov, Accessed: 2022-03-28.

[31]Rumsey, C. L., "The 4th AIAA CFD High Lift Prediction Workshop (HLPW-4): Grids," https://hiliftpw.larc.nasa.gov/Workshop4/grids.html, Accessed: 2022-03-28.

[32]Lee, H. B., Ghia, U., Bayyuk, S., Oberkampf, W. L., Roy, C. J., Benek, J. A., Rumsey, C. L., Powers, J. M., Bush, R. H., Mani, M., "Development and Use of Engineering Standards for Computational Fluid Dynamics for Complex Aerospace Systems," AIAA Paper 2016-3811, June 2016, doi: https://doi.org/10.2514/6.2016-3811.